Supporting Information

for "Directing Anisotropic Assembly of Metallic Nanoclusters by Exploiting Linear Trio Interactions and Quantum Size Effects: Au Chains on Ag(100) Thin Films"

Yong Han and James W. Evans

Department of Physics and Astronomy, and Division of Chemical and Biological Sciences, Ames Laboratory—U. S. Department of Energy, Iowa State University, Ames, Iowa 50011, USA

Density functional theory (DFT) Analysis

Our DFT total energy calculations were performed by using the plane-wave VASP code [1-4] with slab geometries representing the surface. Here, slabs with a specific lateral supercell size (described below) and various arrangements of adsorbates on one side (the "top" side) are repeated periodically in the plane of the slab. In the orthogonal direction, slabs separated by a vacuum region and also repeated periodically. The vacuum thickness between adjacent slabs is always greater than 1.5 nm, which was shown to be thick enough for energy convergence (i.e., to eliminate significant interaction between adjacent slabs). We use the projector augmented wave (PAW) method [5, 6] for the electron-core interactions, and the PBE-GGA [7] for exchange and correlation. The corresponding pseudopotentials (PPs) were generated by the VASP group, and described as the "standard" PPs to differentiate them from newly-released PPs in 2013. The energy cutoffs for the plane wave basis are set to be default values of VASP code (249.846 eV for Au-Ag system, and 269.533 eV for Au-Ag-Ni-Al system). During the optimization/relaxation of atomic positions, the bottommost layer of the slab is always fixed and other atoms are allowed to relax until the self-consistent forces reach the tolerance of 0.1 eV/nm. (Thus, the fixed layer is an Ag layer for the freestanding Ag(100) films, and an Al layer for a 5-ML Al-terminated NiAl(100) slab which is used to support an Ag(100) thin film.) For the fixed layer, and also for the other layers in the slab before relaxation, we use the theoretical lattice constant, $a_{\mathrm{Ag}} = 0.4166$ nm for Ag(100), and $a_{\mathrm{NiAl}} = 0.2896$ nm for NiAl(100). Finally, to assess energetics for Au on bulk Ag(100), DFT results for Ag(100) slabs were averaged over a range of large thicknesses (7-12 ML) which appears to be an effective way to eliminate QSE and to extrapolate to bulk behavior. Selection of supercell size and the corresponding Γ-centered **k** mesh depends on the quantities being analyzed, as described below.

First, we comment on our direct calculation of conventional (ω-) and distinct unconventional (ϕ-) interactions for isolated pairs and triples of adatoms. Here, first pair interactions are determined for all relevant separations. Values for these are obtained from the total system energy, E_{tot}, with a pair of adatoms by subtracting the slab energy and twice the adsorption energy for isolated adatoms, E_{ads}. Then, trio interactions are obtained from E_{tot} with a triple of adatoms by subtracting the slab energy, three times E_{ads}, and also all pair interactions occurring within the triple of adatoms. For this analysis, we use a large lateral supercell size (10×10). The **k** mesh is taken to be 5×5×1. Such calculations are expensive because of the large supercell, in particular for systems with an Ag(100) film supported on a NiAl(100) substrate. After a series of convergence tests with varying

thicknesses of Al-terminated NiAl(100) slabs, we selected a 5-ML slab as the substrate in the Au/Ag(100)/NiAl(100) system. Note that we use an Al-terminated rather than a Ni-terminated NiAl(100) slab since a preference for the Al-termination is broadly recognized [8]. However, actual surface depends on sample preparation and on any slight deviation from stoichiometry in the bulk crystal, and surface defects can occur, e.g., anti-site Ni. Our results show that the strength of the dominant interactions illustrated in Scheme 1 (of a few 10's to 100's of meV) is significantly greater than the strength of the longer-range pair and less compact trio interactions (from a few meV to of the order of ten meV) which can be attractive or repulsive.

As described in the text, we do not use any finite set of these directly calculated DFT values for ω-interactions as the input in our KMC simulations, as such a finite (truncated) set will not exactly recover the key thermodynamic driving force to convert long chains to large 2D adatom islands. Instead, to exactly incorporate this driving force, we use four effective values for ω_{P1}, ω_{P2}, ω_{T1}, and ω_{T2} (see Scheme 1 for these interactions) which are selected to recover exactly the following interaction energies per Au adatom: E_{1D} for a 1D chain, E_{2D} for a 2D 1×1 adlayer, $E_{\mathrm{c(2\times2)}}$ for a c(2×2) adlayer, and E_{square} for an isolated 2×2 adatom square, by solving the equations listed in the text. As an aside, we have checked sensitivity of the resulting values of the four effective ω-interactions to choice of four configurations whose energies are used to determine them. For example, if we retain the 1D chain, 2D 1×1 adlayer, and c(2×2) adlayer, but replace the isolated square by a double chain, we find little change in these values. For the 1D chain, we use a lateral 10×1 supercell with a **k** mesh of 5×35×1. For the 2D 1×1 and c(2×2) adlayer structures, **k** meshes are taken to be 35×35×1, and 21×21×1, respectively. For an isolated 2×2 square island, the lateral supercell size is 10×10 with the **k** mesh of 5×5×1. The above strategy constitutes a standard "cluster expansion" type approach for determining metal adatom interactions [9]. However, we select configurations for DFT analysis to ensure that the effective interactions recover exactly the above-mentioned key system thermodynamics.

Next, we compare results for ω-interactions obtained from direct calculation versus effective values from the cluster expansion approach. Table S1 lists the ω-interaction ratios for Au on 2 - 5 ML Ag(100) films, and Au on 1 - 3 ML Ag(100) films supported on Al-terminated NiAl(100). The superscript "DFT" denotes the ω-interaction value from direct calculations using a large lateral supercell size of 10×10, and the superscript "EFF" denotes the effective ω-interaction values. From Table S1, the ratios $\omega_{\mathrm{P1}}^{\mathrm{EFF}}/\omega_{\mathrm{P1}}^{\mathrm{DFT}}$ and $\omega_{\mathrm{T1}}^{\mathrm{EFF}}/\omega_{\mathrm{T1}}^{\mathrm{DFT}}$ are around 1, indicating the effective values are comparable to those directly from the large-supercell calculations. We should note that the magnitude of values for ω_{P2} and ω_{T1} are significantly smaller than for ω_{P1} and ω_{T2}. Thus, the magnitude of the absolute uncertainty in the DFT prediction of the former is larger, and there is generally a greater deviation between EFF and DFT values.

Now, we briefly comment further on determination of unconventional ϕ-interactions which reflect interaction of a hopping adatom at the bridge site transition state with other nearby adatoms at four-fold-hollow adsorption sites. Focusing on chain or island formation, it should suffice to include just the four dominant ϕ-interactions, ϕ_{P1}, ϕ_{T1}, ϕ_{T2}, and ϕ_{T3}, (shown in Scheme 1 in the text) and neglect other ϕ-interactions. When calculating ϕ-interactions, we specifically fix the x- or y- coordinate (parallel to surface aligned with the

two surface atoms forming the bridge site) of the Au adatom on the bridge site to avoid motion of the adatom towards its neighboring 4-fold-hollow site. This would generally occur due to the asymmetry induced by the local adatom environment.

Table S1. The ω-interaction ratios for Au on unsupported 2 - 5 ML Ag(100) films, and for Au on 1 - 3 ML Ag(100) films supported on Al-terminated NiAl(100).

Ag(100)	$\omega_{\mathrm{P1}}^{\mathrm{EFF}}/\omega_{\mathrm{P1}}^{\mathrm{DFT}}$	$\omega_{\mathrm{T1}}^{\mathrm{EFF}}/\omega_{\mathrm{T1}}^{\mathrm{DFT}}$
2 ML	0.857	1.316
3 ML	1.002	0.808
4 ML	0.872	0.869
5 ML	0.899	1.189
1 ML/NiAl	0.913	1.123
2 ML/NiAl	0.930	0.814
3 ML/NiAl	0.987	1.012

It is appropriate to also note that from analysis using the PBEsol functional [10], we find that interaction energy magnitudes are on average increased by about 20% relative to those determined with the PBE functional. Our previous analysis for the Ag/Ag(100) system suggests that the higher PBEsol values more accurately reflect adlayer interactions in fcc metal systems. Thus, in the KMC simulations reported in the text, the input interactions listed in Table I and Table S1 are obtained by taking the values obtained from extensive PBE analysis and multiplying by a factor of 1.23. The differences between PBE and PBEsol values of interactions, and also the differences between directly calculated versus effective values, prompt the question of whether self-assembly behavior depends strongly on the choice of energetic input to the KMC simulations of Au deposition. In fact, we have performed simulations with three distinct choices of interactions (effective PBEsol, effective PBE, and directly calculated PBEsol). In all choices, we find common trend: chain formation at 250 K and below for lower Au coverages; and 2D island formation at higher temperatures and higher coverages. Some details of these features and their relative prominence for different systems depend on the choice of interactions.

We also performed selected analyses with the newly-updated PAW-PBE PPs (released in 2013) from the VASP group. We obtained a slightly different lattice constant of 0.4152 nm for Ag (cf., the above $a_{\mathrm{Ag}} = 0.4166$ nm), while for NiAl it is 0.2895 nm (almost the same as above $a_{\mathrm{NiAl}} = 0.2896$ nm). Using the updated version of PPs, we also analyzed the adsorption energy difference between bridge and hollow sites to determine E_{d} for Au on Ag(100), and found no significant changes from results with the "standard" PPs. Using PBEsol with updated potentials, we obtain a lattice constant of 0.4054 nm for Ag, and

0.2864 nm for NiAl (cf., experimental values: 0.4069 nm for Ag at 0 K [11, 12], and 0.2887 nm for NiAl at room temperature [13, 14]).

Our modeling did not include exchange of Au with an Ag atom in the top layer of Ag(100) as the associated barrier, E_{ex}, is prohibitively high. For example, for a 1-ML Ag(100) film supported on NiAl(100), we performed analyses using 3×3 and 4×4 supercell sizes using the climbing NEB approach [15, 16] to obtain estimates of the exchange barriers of 0.756 and 0.724 eV, respectively. The slightly lower latter value presumably reflects more facile relaxation of the region surrounding the exchange event for the larger supercell. The **k** mesh is 15×15×1 for both cases. Setting $\delta E = E_{\mathrm{ex}} - E_{\mathrm{d}} \approx 0.28$ eV, this implies a diffusion length $L_{\mathrm{ex}} = ae^{-\delta E/(k_{\mathrm{B}}T)}$ of Au before exchange, where $a \approx 0.289$ nm is the surface lattice constant. This L_{ex} is sufficiently large that Au adatoms aggregate into nanoclusters before exchanging.

Discussion of Quantum Size Effects (QSE) in Ag(100) thin film systems

QSE is relevant for metal-on-metal films as well as metal-on-semiconductor films, since electron confinement is still possible in the former case. As discussed in the text, this confinement can result from various features, e.g., a gap or pseudo gap in the direction normal to the interface, or just a depletion in the density of states of the support near the Fermi level (as expected for NiAl). However, in general one expects a "phase-shift" in the variation of energetics with thickness relative to an unsupported slab. In a simple free electron gas treatment for the film, one solves Schrödinger equation with different boundary conditions at the film-substrate interface for the supported film versus the film-vacuum interface for the slab. This can result in a shift in distinctive features of behavior (e.g., a local minimum in surface energy) to different thickness.

For epitaxial growth by deposition on supported thin films, various effects can contribute to a dependence of the thickness of the supported film. Deconvolution of these effects is in general non-trivial. Specifically, QSE, strain, and chemical bonding variation can all contribute to such a thickness dependence. Strain effects are eliminated in our system due to an excellent lattice match of fcc Au and Ag, and also of Ag(100) and NiAl(100). However, with regard to chemical bonding variation, top layer Ag in supported films is bound below to Al for 1 ML films, but to Ag for ≥ 2 ML films. These different chemical environments which could influence Au adatom interaction energetics. Nonetheless, strong evidence that QSE indeed controls the thickness variation for ≥ 2 ML supported films (where top layer Ag is always bound below to Ag) follows from the similar variation with thickness in Au interaction energies to that observed for unsupported Ag(100) slabs.

More specifically, as shown in Figure S1, while one sees the same trends in variation of the various ω's with thickness, there is a "phase shift" between behavior for unsupported and supported slabs, where the same feature appear for a 1-2 ML greater film thickness for the unsupported relative to the supported films. Analogous behavior is seen in other similar systems, e.g., comparing Ag(100) slabs and supported Ag/Fe(100) films [17].

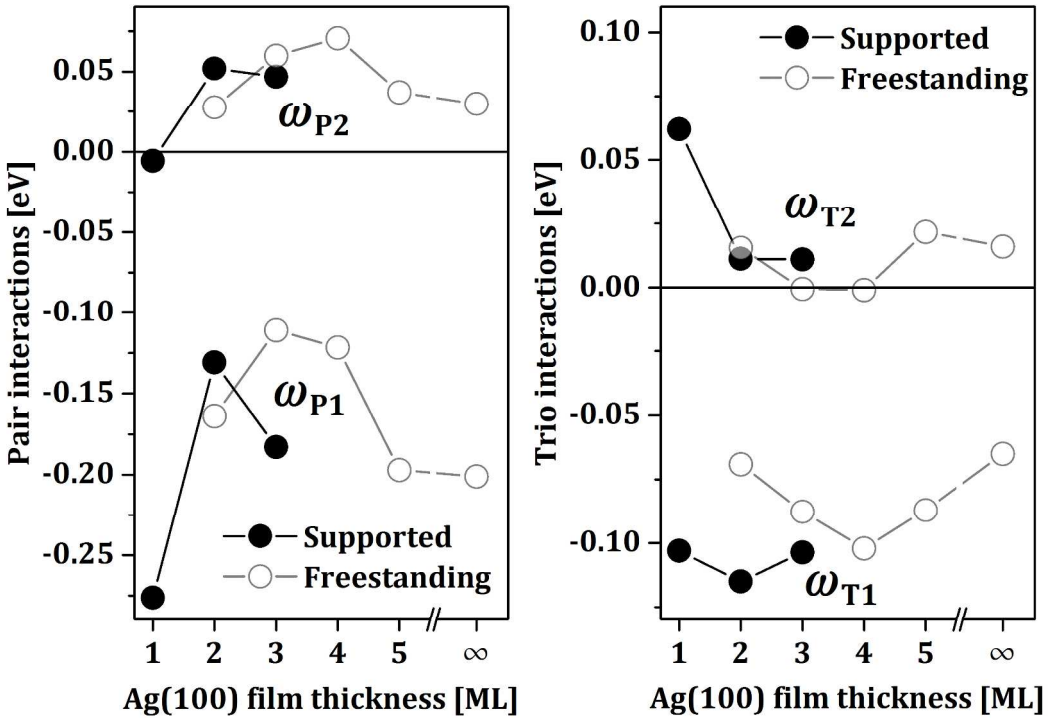

Figure S1. Comparison of the variation with thickness of conventional Au interactions for unsupported Ag(100) slabs and supported Ag(100) films on Al-terminated NiAl(100). Note that the same general trends appear, but with a "phase shift" to 1-2 ML greater film thickness for the unsupported slab.

Kinetic Monte Carlo (KMC) simulation algorithm

We briefly describe our KMC simulation algorithm which is consistent with the prescribed stochastic lattice-gas model for the deposition and diffusion-mediated self-assembly of Au nanoclusters on Ag(100) thin films. The basic requirement of the algorithm is simply to implement various processes (deposition, hopping of adatoms between neighboring four-fold-hollow sites in various local environments) with probabilities proportional to their physical rates. The rate of deposition per site is a constant, F. The numerous rates for adatom hopping are given by the generic formula $h = \nu e^{-E_{\rm act}/(k_{\rm B}T)}$ with $E_{\rm act} = E_{\rm d} + \Phi_{\rm TS} - \Phi_{\rm init}$. Here $\Phi_{\rm init}$ ($\Phi_{\rm TS}$) is determined from summing appropriate ω- (ϕ-) interactions, as described in the text. The simulation approach implemented is a Bortz-Kalos-Lebowitz (BKL)-type rejection-free algorithm [18].

Our BKL-type algorithm for deposition and diffusion-mediated assembly is implemented for a system with $L \times L$ surface adsorption sites, which are labeled (i, j), and periodic boundary conditions. We determine the total deposition rate $R_{\rm dep} = FL^2$, and track the total hopping rate $R_{\rm hop} = \sum_{k=1}^{N_{\rm hop}} R_k$, where $N_{\rm hop}$ is the number of adatoms which can potentially hop (if they are not surrounded by four occupied sites), and R_k is the total hop rate for the $k^{\rm th}$ such adatom. Thus, the total rate for all processes in the system is $R_{\rm tot} = R_{\rm dep} + R_{\rm hop}$, and this changes during the simulation since $R_{\rm hop}$ changes. A random number, ξ, is selected uniformly distributed on [0,1]. If $\xi < R_{\rm dep}/R_{\rm tot}$, one implements

deposition, and otherwise hopping. For the former, one randomly selects one of the L^2 adsorption sites, (i, j), with the aid of two random numbers (one to select i and the other j). If hopping is selected, another random number, ξ, is selected. If $R_1 + R_2 + \cdots + R_{k-1} < \xi R_{\text{hop}} \leq R_1 + R_2 + \cdots + R_k$, one selects the k^{th} adatom for hopping. Then, one must select one of up to four possible directions ($\alpha = 1$, 2, 3, or 4) to move this adatom. If the corresponding hop rates are $R_k(\alpha)$, a random number ξ is selected, and the direction of hopping is chosen as $\alpha = 1$ if $\xi R_k \leq R_k(1)$, as $\alpha = 2$ if $R_k(1) < \xi R_k \leq R_k(2)$, etc. In our simulation, it is not particularly important to track physical time as typically we run the simulation until a specified amount of Au is deposited. However, time, t, is readily tracked, being incremented by an amount $\Delta t = -\ln(\eta)/R_{\text{tot}}$ for each deposition or hopping event, where η is a random number uniformly distributed on [0,1].

REFERENCES

[1] Kresse, G.; Hafner, J. *Phys. Rev. B* **1993**, *47,* 558.

[2] Kresse, G.; Hafner, J. *Phys. Rev. B* **1994**, *49,* 14251.

[3] Kresse, G.; Furthmüller, J. *Comput. Mat. Sci.* **1996**, *6*, 15.

[4] Kresse, G.; Furthmüller, J. *Phys. Rev. B* **1996**, *54,* 11169.

[5] Blochl, P. E. *Phys. Rev. B* **1994**, *50*, 17953.

[6] Kresse, G.; Joubert, D. *Phys. Rev. B* **1999**, *59,* 1758.

[7] Perdew, J. P.; Burke, K.; Ernzerhof, M. *Phys. Rev. Lett.* **1996**, *77,* 3865.

[8] Lerch, D.; Dössel, K.; Hammer, L.; Müller, S. *J. Phys.: Condens. Matter* **2009**, *21,* 134007.

[9] Stasevich, T. J.; Einstein, T.L; Stolbov, S. *Phys. Rev. B* **2006,** *73,* 115426.

[10] Perdew, J. P.; Ruzsinszky, A.; Csonka, G. I.; Vydrov, O. A.; Scuseria, G. E.; Constantin, L. A.; Zhou, X.; Burke, K. *Phys. Rev. Lett.* **2008,** *100,* 136406.

[11] Giri A. K.; and Mitra, G. B. *J. Phys. D: Appl. Phys.* **1985**, *18,* L75.

[12] Shoenberg, D. *Phil. Trans. R. Soc. Lond. A* **1962**, *255,* 85.

[13] Noebe, R. D.; Bowman, R. R.; Nathal, M. V. *Int. Mater. Rev.* **1993,** *38,* 193.

[14] Taylor, A.; Doyle, N. J. *J. Appl. Cryst.* **1972,** *5*, 201.

[15] Henkelman, G.; Uberuaga, B. P.; Jónsson, H. *J. Chem. Phys.* **2000**, *113,* 9901.

[16] Henkelman, G.; Jónsson, H. *J. Chem. Phys.* **2000**, *113,* 9978.

[17] Wei, C. M.; Chou, M. Y. *Phys. Rev. B* **2003**, *68*, 125406.

[18] Bortz, A. H.; Kalos, M. H.; Lebowitz, J. L. *J. Comp. Phys.* **1975**, *17,* 10.